# Twisted superconducting quantum diodes: Towards anharmonicity and high fidelity

Han Zhong<sup>1</sup>, Denis Kochan<sup>2,3</sup>, Igor Žutić<sup>4</sup>, and Yingying Wu\*<sup>1</sup>

<sup>1</sup>Department of Electrical and Computer Engineering, University of Florida, Gainesville, FL 32611, USA

<sup>2</sup>Department of Physics and Center for Quantum Frontiers of Research and Technology (QFort), National Cheng Kung University, Tainan 70101, Taiwan <sup>3</sup>Institute of Physics, Slovak Academy of Sciences, 84511 Bratislava, Slovakia <sup>4</sup>Department of Physics, State University of New York at Buffalo, Buffalo, New York 14260, USA

#### **Abstract**

As quantum technologies advance, a fundamental challenge is mitigating noise and backscattering in superconducting circuits to achieve scalable, high-fidelity operations. Conventional superconducting components lack directionality, causing energy loss and decoherence. Superconducting diodes—that allow dissipationless current in one direction and resistive flow in the other—offer a potential remedy, yet their efficiency and quantum integration remain limited. Here, we realize a quantum diode in twisted NbSe<sub>2</sub> bilayers under in-plane and out-of-plane magnetic fields. A mere 1° twist yields an efficiency enhancement over pristine devices, reaching 27.6%. Quantum simulations reveal that this intermediate efficiency—well below 100% ideal—is both experimentally practical and optimal for preserving qubit anharmonicity and stabilizing two-level systems. These findings show that maximal rectification is not always beneficial for quantum information, establishing a new principle for designing the fundamental properties of twisted superconductors towards low-power, high-fidelity quantum circuits.

<sup>\*</sup>Corresponding author: yingyingwu@ufl.edu

## Introduction

Superconducting diodes unify the dissipationless properties of superconductivity with the unidirectional current flow of traditional semiconductor diodes [1, 2]. Similar to how semiconductor diodes exhibit nonreciprocal resistive charge transport, superconducting diodes demonstrate nonreciprocity in the superconducting state, allowing superconducting currents to flow preferentially in one direction while being suppressed in the opposite direction. This behavior arises from a combination of symmetry-breaking mechanisms, such as spin-orbit coupling, applied magnetic fields, or intrinsic material properties [2]. By integrating key superconducting characteristics-such as zero electrical resistance, low noise, and high coherence [3] with the directional control of current flow, superconducting diodes hold transformative potential for energy-efficient computing architectures, to enable superconducting logic and memory elements with minimal power dissipation, as well as support ultrafast operation, including THz applications [4–6]. Furthermore, superconducting diodes offer exciting prospects for quantum sensing and ultra-sensitive magnetometry [3], by exploiting their nonreciprocal superconducting transport properties [1].

Recent studies show that the superconducting diode effect can be realized in both Josephson junctions and junction-free superconductors [1, 7]. Related advances are usually characterized by the efficiency of a superconducting diode which is defined as the difference between the critical currents,  $I_C$ , in the forward, and reverse directions, normalized by their sum [1, 8, 9]

$$\eta = \frac{|I_C^+| - |I_C^-|}{|I_C^+| + |I_C^-|} \times 100\%,\tag{1}$$

where  $I_C^+$  ( $I_C^-$ ) denotes the critical current in the forward (reverse) direction. The form of Eq. (1) is analogous to the expression for spin polarization or magnetoresistance, enhancing their values characterizes the improved performance of spintronic spin-valve devices [10]. The push towards a high-diode efficiency is further motivated by the prospect that in van der Waals (vdW) heterostructures their atomically sharp interfaces could lead to high on/off ratios exceeding those in the common spintronic spin-valve devices. Experimental diode efficiency in vdW heterostructures [11] is comparable to the state-of-the art values  $\eta \sim 70\%$  in sputtered materials and their heterostructures [4, 7]. An additional advantage of vdW heterostructures based on high-temperature superconductors [12] is that a large  $\eta \sim 50\%$  can be maintained at higher operating temperature than in superconducting diodes from sputtered materials. To date, the superconducting diodes have been proposed primarily for their use as current rectifiers [1, 13], which explains the primary focus on enhancing the corresponding  $\eta$ . A similar trend in  $\eta$  can be also seen from the concept of a quantum diode designed for the integration with of solid-state qubits and characterized by transport nonreciprocity, enabling unidirectional excitation transfer between the boundary resonators of a lattice. The quality of the quantum diode is characterized by its fidelity, which can be improved by increasing  $\eta$ , when the one-way excitation transfer process becomes more pronounced [14].

However, how the diode efficiency influences much broader functionalities remains poorly understood, but it is essential to unlock their full potential. Surprisingly, our work on vdW twisted superconducting quantum diodes reveals that an *intermediate*, experimentally realized, and not ideal efficiency of  $\eta \to 100\%$  can enable their optimal performance. Such twisted systems offer a platform to study fundamental phenomena and the interplay between time-reversal symmetry breaking, topology, spin-orbit coupling, and strongly-correlated effects [11, 12, 15].

Here we explore the twisted layers of vdW superconductor NbSe<sub>2</sub> and report  $\eta=27.6\%$ . A twist angle of just 1°, enhances  $\eta$  nearly an order of magnitude from a pristine NbSe<sub>2</sub> [16], while the spontaneously broken-time reversal symmetry leads to the diode effect even in the absence of an applied magnetic field. Guided by the measured  $\eta$ , we simulate a novel scalable quantum diode design that provides strong anharmonicity for qubit operations and enables seamless integration into quantum circuits. Our approach elucidates the role of  $\eta$  on quantum functionalities

and reexamines the integration of superconducting diodes into a growing landscape of quantum architectures.

# **Diode Design**

NbSe<sub>2</sub> is a transition metal dichalcogenide which, with a weak interlayer vdW bonding, allows its exfoliation into thin flakes or even monolayers. A strong intrinsic spin-orbit coupling of a monolayer NbSe<sub>2</sub> pins the spins of electrons with opposite momenta to opposite out-of-plane direction. In the superconducting state such a spin-momentum locking favors Ising pairing [17– 19], the formation of singlet-like Cooper pairs with electrons spins pinned perpendicular to the monolayer, and protects the pairs against in-plane spin polarization, withstanding a much large in-plane B. We have fabricated twisted NbSe<sub>2</sub> structure using a twist angle of 1° since the reconstruction appears to be particularly strong when the twist angle is less than 1.2° [20]. Figure 1a presents a schematic representation of a twisted bilayer NbSe<sub>2</sub> system with a twist angle of  $\theta$  and Fig. 1b is its corresponding electrical characterization setup with four terminals. The temperaturedependent resistance measurement reveals a superconducting transition at a critical temperature of 6.87 K. The inset of Fig. 1c presents a false color image of the fabricated NbSe<sub>2</sub> device, highlighting different regions and components involved in the electrical characterization. Yellow and green parts represent, respectively, the gold electrodes and the h-BN encapsulation layer, which is preventing the oxidation and degradation of the NbSe<sub>2</sub> layers. The dark layer corresponds to the twisted NbSe<sub>2</sub> layers, whose superconducting properties are the focus of the work. Prior studies of superconductivity in twisted multilayers include other vdW materials such as graphene [15, 21] and high-temperature superconductor, Bi<sub>2</sub>Sr<sub>2</sub>CaCu<sub>2</sub>O<sub>8+x</sub> [12], but NbSe<sub>2</sub>-based superconducting diodes were largely explored without any twist angle [1, 2].

## **Results on critical currents and diode effect**

While NbSe<sub>2</sub>-based superconducting diodes exhibit at B=0 a vanishing rectification efficiency [2], our measurements yield  $\eta\approx-2.1\%$ . This indicates a finite intrinsic anisotropy in the device under applied magnetic fields below  $10^{-4}$  T, as shown in Fig.1d. This can be attributed to an emergent correlated phase surviving weak fields that possess a spontaneous twist-induced magnetization stemming from a combination of strong electronic interactions, underlying moiré landscape and a non-trivial band topology. Their interplay can give rise to a state with orbital magnetization and thus spontaneously broken time-reversal symmetry as reported for nonmagnetic vdW materials with small twist angles [22]. However, applying an out-of-plane B, Fig. 1e, modulates the resistance, demonstrating the field's influence on superconducting properties. Similarly, resistance measurements under varying in-plane B, Fig. 1f, displays magnetochiral response, further emphasizing the role of external magnetic fields in tuning the electronic properties of the twisted NbSe<sub>2</sub> system. These findings indicate spin-orbit coupling-affected superconductivity [2], possibly an unconventional Ising pairing due to the characteristic vdW spin-momentum locking.

After fabricating twisted NbSe<sub>2</sub> devices with three representative overall thicknesses–16 nm, 30 nm, and 60 nm (corresponding to 8 nm, 15 nm, and 30 nm per NbSe<sub>2</sub> layer)–and performing resistance-temperature (R-T) measurements, we further investigate their current-voltage (I-V) characteristics under both in-plane and out-of-plane  $\boldsymbol{B}$ . Figure 2 shows the I-V curves and diode efficiencies under varied magnetic field directions and strengths. Our measurements demonstrate  $\boldsymbol{B}$ -dependent nonreciprocal transport behavior, essential for the superconducting diode effect.

Figures 2a-c, show I-V curves for the device with overall thickness of 16 nm in the in-plane  $B=\pm 20\,\mathrm{Oe}$  and  $\pm 180\,\mathrm{Oe}$  applied (anti)parallel to the current with the maximum  $\eta\approx 24.0\%$  at -100 Oe. Variations in the I-V curves indicate that inversion symmetry is broken in the superconducting state, while the observation of the diode effect along the current points, according to theory developed in [23], to the possibility of interfacial spin-orbit coupling texture with a non-zero radial Rashba component as also supported by density functional theory calculations in similar vdW materials with a twist [24, 25]. Correspondingly, Figs. 2d-f, display I-V curves under an out-of-

plane B at  $\pm 2$  Oe and  $\pm 20$  Oe with the maximum  $\eta \approx 27.6\%$  at -13 Oe, demonstrating a strong nonreciprocal response with an only small perpendicular field. This suggests that the system experiences the vortex diode effect [26] as also observed in other systems [7, 27, 28] in out-of-plane B. Twisting the two NbSe<sub>2</sub> layers creates an asymmetry between its edges that impacts on different heights of the associated Bean-Livingston surface barriers [29], and hence on different onsets of the resistive states depending on the polarity of current drive, or an out-of-plane B [13, 30, 31].

Figures 2g-h show representative I-V curves measured at out-of-plane  $B=\pm 20$  Oe for devices with an overall thickness of 30 nm and 60 nm. In both cases, a clear nonreciprocity is observed in the I-V responses, with asymmetry in the forward and reverse critical currents. Figure 2i summarizes  $\eta$  as a function of out-of-plane B for junctions of different thicknesses. The 16 nm device exhibits a pronounced B-dependent diode efficiency, while the 30 nm and 60 nm devices show a much weaker nonreciprocal behavior highlighting the role of interlayer coupling and symmetry breaking in controlling the rectification effect. The thickness dependence of the nonreciprocity originates from the vortex diode effect: in thicker samples, the Meissner screening current density is reduced and the effective Pearl penetration depth,  $\lambda_{\text{Pearl}} = \lambda_{\text{London}}^2/d$ , becomes smaller, which in turn enhances the asymmetry of the Bean–Livingston vortex surface barriers, where  $\lambda_{\text{London}}$  is the London penetration depth [3] and d is the sample thickness. Consequently, in thicker samples the vortices are bounded to the edges more firmly than in the thinner films, what suppresses transition into the resistive state. These results demonstrate the tunability of the superconducting diode effect in twisted NbSe<sub>2</sub> bilayers through external magnetic fields, with distinct optimal field values for inplane and out-of-plane configurations. This behavior suggests an interplay between moiré-induced electronic states, interfacial coupling phenomena, and vortex diode effect, altogether influencing the transport properties of the twisted NbSe<sub>2</sub> bilayers.

The behavior of twisted NbSe<sub>2</sub> bilayers under different orientations of the in-plane  $\boldsymbol{B}$  reveals distinct dependencies of the diode effect on a mutual orientation of the field and current drive. Figure 3 shows schematics and experimental results of the critical currents and  $\eta$  for a device with an overall thickness of 16 nm, exposed to the in-plane magnetic  $\boldsymbol{B}$  parallel (Figs. 3a-c) and perpendicular (Figs. 3d-f) to the current. A similar analysis is performed also in the case when angle between the in-plane  $\boldsymbol{B}$  and current is arbitrary (Figs. 3g-i). In all three cases the corresponding critical currents and diode efficiencies indicate a strong directional dependence of superconducting transport, where the orientation of the in-plane  $\boldsymbol{B}$  significantly influences the nonreciprocal supercurrent behavior. These results highlight the role of twisting and spin-orbit coupling engineering at the interface of two NbSe<sub>2</sub> layers that, correspondingly, imparts the anisotropic superconducting diode effect features sensed by the in-plane  $\boldsymbol{B}$ .

The error bars for critical currents were calculated using bootstrap resampling [32], that estimates uncertainty without assuming a specific probability distribution. The process involves repeatedly drawing random samples with a replacement from the original I-V measurements near the critical point. In the code, this is implemented with 100 resamplings for each critical current determination, sampling from a window of up to 11 data points (5 on each side of the detected critical point). For each resampled dataset, the critical current is recalculated using the same voltage gradient method as applied to the original data. The standard deviation of these 100 recalculated critical currents provides a robust estimate of measurement uncertainty, revealing how the critical current determination might vary with slightly different experimental data points. For the analysis of  $\eta$ , its sinusoidal relationship with an applied B is modeled as  $\eta = a \sin(b B + c)$ , where a and b parametrize the amplitude and frequency, while c determines the phase shift. The fitting algorithm employs weighted least squares minimization. By weighting each data point according to its uncertainty, the fit gives greater influence to more reliable measurements. The resulting high coefficient of determination, denoted as  $R^2$  (typically >0.93 in this case), confirms that the sinusoidal model effectively captures the fundamental physics of the B-dependent diode behavior.

# Quantum simulations: A one-way transfer of qubits

After characterizing the rectification properties of the twisted NbSe<sub>2</sub> bilayers, we designed superconducting circuits incorporating such nonreciprocal elements, and simulated their quantum diode characteristics. Leveraging a widely used, gate-based simulation framework of QuTip, an open-source Python framework for simulating open quantum system dynamics [33], we integrated diode efficiency  $\eta$  as a new degree of freedom that is capable to tune the nonreciprocity of the the quantum diode. Figure 4a shows a schematics of nonreciprocal circuit based on the NbSe<sub>2</sub> bilayer junction: Cooper pairs flow with minimal dissipation in the forward direction, while they break into quasiparticles for the reverse bias and thus turning a circuit into a resistive state. Figure 4b depicts particular platform utilizing transmon qubits  $(Q_1, Q_2, Q_3)$  interconnected by the NbSe<sub>2</sub>-based Josephson junction  $J_1$ ,  $J_2$  (marked by " $\boxtimes$ " symbols). This provides both, the nonlinearity that is essential for the transmon qubits [3], but also an intrinsic supercurrent nonreciprocity. Such built-in directionality not only preferentially steers supercurrents, but also suppresses backward excitations, thereby enhancing a qubit control.  $(Q_1, Q_2, Q_3)$  are individually voltage-biased  $(V_1, V_2, V_3)$  and share a common inductor on the left, enforcing unidirectional quantum-information flow, crucial for isolating signals and preventing backscattering in a scalable and highly-coherent way. Additionally, Fig. 4c compares  $\eta$  across various reported vdW platforms. Highlighted in red, our twisted NbSe<sub>2</sub> devices strike a balance between the rectification strength and critical current.

We next discuss potential ramifications that these nonreciprocal elements can bring to quantum circuits and superconducting qubits. Having any current-phase relation (CPR) [2, 34]  $I(\varphi) = I_J f(\varphi) = I_J \frac{d}{d\varphi} F(\varphi)$ —that possesses non-zero anomalous phase  $\phi_0$  and a skewness leading to the diode nonreciprocity [2],  $I_c^+ = \max_{\varphi} I(\varphi) \neq |\min_{\varphi} I(\varphi)| = |I_c^-|$  – the circuit quantum electrodynamics Hamiltonian,  $\hat{H}$ , for the capacitively shunted Josephson junction is [35]:

$$\hat{H} = 4E_C(\hat{n} - n_q)^2 + E_J F(\hat{\varphi}), \qquad (2)$$

where  $E_C=e^2/(2C)$ , and  $E_J=\Phi_0I_J/2\pi$  are, respectively, the charging (capacitative) and Josephson (inductive) energies, with C the relevant circuit capacitance,  $\Phi_0=h/2e$  the flux quantum, and  $n_g$  a gate-induced charge offset [3], while our generalized  $F(\varphi)$  deviates from the standard  $\cos(\varphi)$  form. Introducing bosonic lowering and raising operators  $\hat{a}$  and  $\hat{a}^\dagger$  for an addition and removal of the Cooper pair, the canonically conjugated phase and number operators are  $\hat{\varphi}=(2E_C/E_J)^{1/4}\,(\hat{a}^\dagger+\hat{a})$  and  $\hat{n}=(i/2)\,(E_J/2E_C)^{1/4}\,(\hat{a}^\dagger-\hat{a})$ , with  $[\hat{\varphi},\hat{n}]=i$  [3]. For simplicity we assume that both junctions  $J_1$  and  $J_2$  are identical and governed by the minimally skew-symmetric CPR with  $f(\varphi)=\sin{(\varphi-\arcsin{\eta})}+\eta$ , or correspondingly,  $F(\varphi)=-\cos{(\varphi-\arcsin{\eta})}+\eta\varphi$ , where  $\eta$  is directly the diode efficiency.

To proceed further, we recall that a superconducting circuit needs a nonlinear element to function as a qubit, while for isolating a controllable two-level system it is important to have an inherent anharmonicity. We focus on a commercially successful transmon qubit with  $E_J\gg E_C$  [3, 35], where the Josephson tunneling dominates, the phase-variable takes a well-defined and minimally uncertain value  $\langle \hat{\varphi} \rangle$  while, desirably, the resulting energy levels are still largely insensitive to fluctuations in  $n_g$ , but the cost of this protection from the charge noise is the reduced anharmonicity [3]. For common transmons, denoting by 0,1,2 its lowest states, the qubit transition frequency and the anharmonicity are, respectively,  $\omega_{01}=(\sqrt{8E_JE_C}-E_C)$  and  $\omega_{12}-\omega_{01}=-E_C/\hbar$  [3]. This analysis of common transmons can be generalized for our case where one expands the underlying goniometric functions entering  $F(\varphi)$  around  $\langle \hat{\varphi} \rangle$  and gets effective qubit Hamiltonian,  $\hat{H}$ , in the truncated space; in the case of our CPR this leads to  $\langle \hat{\varphi} \rangle \equiv 0$  and the truncated Hamiltonian  $\hat{H}$  is

$$\hat{H} \simeq 4E_C(\hat{n} - n_g)^2 + E_J \left[ \frac{1}{2!} \sqrt{1 - \eta^2} \varphi^2 + \frac{1}{3!} \eta \varphi^3 - \frac{1}{4!} \sqrt{1 - \eta^2} \varphi^4 \right]. \tag{3}$$

In the above expression we have disregarded numerical constants that are just globally shifting the origin of energy. The transmon Hamiltonian explicitly breaks the time-reversal and inversion symmetries and therefore the dynamics of the Cooper pairs displays nonreciprocal features. OuTiP is employed to numerically simulate the potential energy landscape of a transmon diode as a function of phase difference under varying diode efficiency. As shown in Fig. 4d, the two-level qubit states—the ground "0" and first excited "1"—in the tilted cosine-like potential are identified and characterized through this simulation. The effective potential exhibits a rich spectrum and wide tunability with respect to  $\varphi$  and  $\eta$ . A narrow operational regime supporting exactly two quantum states within the central potential well can be created through a precise tuning of  $\eta$ . For this analysis, the careful parameter optimization,  $\eta \approx 27.6\%$  and  $E_J/E_C = 20.0$ , is set to maintain consistency with the experimental observations. We find that an intermediate value of  $\eta$ , not 100%, remains also optimal for other ratios  $E_J/E_C$ . Typically, for a larger  $E_J/E_C$  a larger  $\eta$  would lead to the optimal two-level system configuration. Additional analysis on how  $\eta$  value can affect the system is discussed in the Supplementary Information. The resulting potential landscape, depicted by the black curve in Fig. 4d, reveals a characteristic asymmetric multi-well configuration that arises from the complex interplay between the Josephson coupling energy and the phase bias introduced by the diode element. Figure 4d displays three distinct potential profiles corresponding to different diode efficiencies:  $\eta = 10\%$  (left),  $\eta = 27.6\%$  (center), and  $\eta = 50\%$  (right), each spanning a phase range from  $-2\pi$  to  $2\pi$ . The quantized energy eigenstates are represented as discrete horizontal lines overlaid on each potential well, with the two lowest-energy bound states highlighted in red and blue. These states remain spatially localized within the central potential valley and are energetically separated from higher-lying continuum states by the surrounding potential barriers. This evolution demonstrates how different  $\eta$  values systematically modify the energy states:  $\eta = 10\%$  supports three bound states in the potential well,  $\eta = 27.6\%$  maintains exactly two bound states, while  $\eta = 50\%$  has only one bound state. The range of  $\eta$  that is supporting only two-level configuration is found to be particularly advantageous for quantum computing implementations as it suppresses transitions to higher excited states. This can be beneficial for extending the qubit coherence time and, generally, for novel qubit architectures.

To quantitatively assess the performance of the quantum diode, we introduce the concept of fidelity as a direct measure of transport outcomes. The forward (reverse) fidelity quantifies the accuracy with which an excitation is ultimately transferred in the forward (reverse) direction. Figure 4e compares the forward and reverse transport fidelity across the parameter space of  $\eta$  and evolution time, with the upper panels showing ideal noiseless evolution and the lower panels incorporating comprehensive noise models. The fidelity between the two states is calculated using the equation  $F(|\psi\rangle, |\phi\rangle) = |\langle\psi|\phi\rangle|^2$ , where  $|\psi\rangle$  and  $|\phi\rangle$  represent the two quantum states of interest. The noiseless simulations (upper panels), the transport fidelities exhibit sharp, well-defined features with maximum forward fidelity approaching unity and minimum reverse fidelity near zero, creating clear high-contrast regions that demonstrate ideal diode behavior with perfect directional selectivity. The noise implementation includes multiple relevant sources: Parameter fluctuations of  $\pm 0.5$  in  $E_J$ , charge noise with amplitude 0.03 representing Cooper pair number fluctuations, phase noise of amplitude 0.02 from flux variations, energy dissipation at rate 0.01 modeling environmental coupling, and measurement uncertainty of  $\pm 0.002$ . Despite these realistic noise sources, the characteristic transport asymmetry remains clearly visible, as demonstrated in Fig. 4f which shows the overall fidelity difference between forward and reverse directions. The noise primarily introduces broadening and a slight reduction in the peak fidelity values but preserves the fundamental diode behavior, with maximum asymmetry in two levels occurring around  $\eta \approx 22.9\%$ -44.8% and 67.1%-77.4% for evolution times of 1-10 ns (see Supplementary Information). The comparison validates that the quantum diode effect is sufficiently robust for practical quantum circuit applications, maintaining directional transport characteristics even under typical experimental noise levels, where the signal-to-noise ratio exceeds 10:1 in the optimal parameter regime.

# **Conclusion**

In contrast to the current push to maximize the diode efficiency in superconducting diodes and their quantum counterparts, we reveal a much richer picture for optimizing their performance and obtaining functionalities that are not limited to the usual rectifying behavior. Instead of the efforts to design materials and systems which could attain a much higher on/off ratios and  $\eta \to 100\%$ , we put forth a different approach in which already experimentally attained diode efficiency could offer a superior performance of superconducting quantum circuits. Surprisingly, our findings reveal that even a moderate diode efficiency of 27.6% in twisted quantum diodes is already sufficient to stabilize a well-defined two-level system, a fundamental requirement for reliable qubit operation. This level of nonreciprocity enables a high-fidelity quantum state transport by effectively suppressing backscattering and decoherence pathways. A novel quantum diode could also be designed where the qubit states define discrete quantized conduction states, introducing unexplored functionalities for quantum information storage and processing. The anharmonicity in this quantum diode design is particularly well suited for integration with transmon-based quantum circuits [36], characterized by  $E_J/E_C \gg 1$  and weakly anharmonic energy levels to prevent unwanted transitions between higher excited states during quantum operations [3, 35]. We show that in our twisted vdW heterostructures a large tunability of the key parameters determines the energy landscape and transform the qubit's properties to overcome the usual reduction of anharmonicity by introducing controlled anharmonicity in the quantum diode. This compatibility with transmons can enhance their coherence and control fidelity, making the diode a favorable component for hybrid quantum systems. Such a device could advance quantum computing by enabling precise and energy-efficient data retention. However, the studied rectifying properties may also improve operation of other superconducting qubits, beyond transmons. To realize this vision, further experimental research is necessary to fabricate and test various quantum diodes and their tunability, including a tantalizing prospect that the resulting Josephson junctions can be turned on and off in the absence of any bias current, while the resulting anharmonicity could be desirable for neuromorphic computing [5]. The next critical step will be the integration of these diodes into practical quantum circuits, unlocking many possibilities in quantum-enhanced electronics and computation.

Given the complexity of materials for quantum diodes and a growing class of candidates that are building blocks for the resulting vdW heterostructures, machine learning techniques are being explored to accelerate their materials discovery and interface optimization [37–39]. Using AI-driven approaches could predict and design materials combinations to minimize losses and enhance efficiency, making quantum diodes viable for energy-efficient and noise-resilient quantum circuits. Conversely, a similar approach would also enable exploring a large phase space of materials parameters and the discovery of fundamental properties in twisted superconducting diodes. Given that diode effects can characterize Josephson junctions [8] and accompany topological superconductivity [2], there is an intriguing prospect of using diode effects in exploring topological superconductivity in twisted vdW systems.

## **Methods**

#### Device fabrication

Pristine NbSe<sub>2</sub> are commercially bought from a company. The thin films are obtained from mechanical exfoliation using conventional scotch tape. The metal electrodes are prepared using photolithography, followed by e-beam evaporation of 5 nm/30 nm Cr/Au films. The heterostructures were assembled using transfer stage, with assistance of PDMS/PPC polymers to hold the layers. After the assembly of the heterostructure, all layers were transferred onto the prepared metal electrodes, then using acetone to remove polymer layers.

#### Transport measurement

Four-probe geometry current vs voltage scans were measured to observe the critical current nonreciprocity. The measurement was done in our Physical Property Measurement System (PPMS) with a temperature range of 1.6 K-400 K and a magnetic field of  $\pm 9$  T. A DC source is applied

from Keithley 2450 and Keysight B2902A.

## QuTip quantum simulation

The quantum simulation presented in this study utilizes the Quantum Toolbox in Python (QuTiP), a robust open-source software designed specifically for quantum mechanics and quantum computing simulations. QuTiP allows efficient numerical calculations involving quantum states, density matrices, Hamiltonians, and time evolutions, making it particularly suitable for modeling complex quantum systems such as the multi-qubit quantum diode discussed herein. In this simulation, QuTiP facilitates the representation and manipulation of quantum states with Josephson junction providing the diode efficiency, the implementation of time evolution operators, and the inclusion of realistic quantum noise and decoherence effects. By leveraging QuTiP's powerful computational tools, the forward and backward quantum state transfer probabilities were systematically explored under varying levels of coupling asymmetry and noise conditions, accurately capturing the dynamics essential for analyzing quantum diode performance.

## **Data Availability**

The data are available in UF QESI webpage under the "Research and Data Sharing".

### References

- 1. Nadeem, M., Fuhrer, M. S. & Wang, X. The superconducting diode effect. *Nature Review Physics* **5**, 558–577 (2023).
- 2. Amundsen, M., Linder, J., Robinson, J. W., Žutić, I. & Banerjee, N. Colloquium: Spin-Orbit Effects in Superconducting Hybrid Structures. *Review of Modern Physics* **96**, 021003 (2024).
- 3. Tafuri (ed.), F. Fundamentals and Frontiers of the Josephson Effect (Springer Nature, Cham, 2019).
- 4. Golod, T. & Krasnov, V. M. Demonstration of a superconducting diode-with-memory, operational at zero magnetic field with switchable nonreciprocity. *Nature Communications* **13**, 3658 (2022).
- 5. Monroe, D., Shen, C., Tringali, D., Alidoust, M., Zhou, T. & Žutić, I. Phase jumps in Josephson junctions with time-dependent spin-orbit coupling. *Applied Physics Letters* **125**, 012601 (2024).
- 6. Yang, C.-J., Li, J., Fiebig, M. & Pal, S. Terahertz control of many-body dynamics in quantum materials. *Nature Reviews Materials* **8,** 518–532 (2023).
- 7. Hou, Y. *et al.* Ubiquitous superconducting diode effect in superconductor thin films. *Physical Review Letters* **131**, 027001 (2023).
- 8. Pekerten, B., Brandão, D. S., Bussiere, B., Monroe, D., Zhou, T., Han, J. E., Shabani, J., Matos-Abiague, A. & Žutić, I. Beyond the standard model of topological Josephson junctions: From crystalline anisotropy to finite-size and diode effects. *Applied Physics Letters* **124**, 252602 (2024).
- 9. Cuozzo, J. J., Pan, W., Shabani, J. & Rossi, E. Microwave-tunable diode effect in asymmetric SQUIDs with topological Josephson junctions. *Physical Review Research* **6**, 023011 (2024).
- 10. Žutić, I., Fabian, J. & Das Sarma, S. Spintronics: Fundamentals and applications. *Reviews Modern Physics* **76**, 323–410 (2004).
- 11. Lin, J.-X. *et al.* Zero-field superconducting diode effect in small-twist-angle trilayer graphene. *Nature Physics* **18,** 1221–1227 (2022).

8

- 12. Zhao, S. F. *et al.* Time-reversal symmetry breaking superconductivity between twisted cuprate superconductors. *Science* **382**, 1422–1427 (2023).
- 13. Ingla-Aynés, J., Hou, Y., Wang, S., Chu, E.-D., Mukhanov, O. A., Wei, P. & Moodera, J. S. Efficient superconducting diodes and rectifiers for quantum circuitry. *Nature Electronics* **8**, 411–416 (2025).
- 14. Zhao, X., Xing, Y., Cao, J., Liu, S., Cui, W.-X. & Wang, H.-F. Engineering quantum diode in one-dimensional time-varying superconducting circuits. *npj Quantum Information* **9**, 59 (2023).
- 15. Cao, Y., Fatemi, V., Fang, S., Watanabe, K., Taniguchi, T., Kaxiras, E. & Jarillo-Herrero, P. Unconventional Superconductivity in Magic-angle Graphene Superlattices. *Nature* **556**, 43–50 (2018).
- 16. Zhang, Y. *et al.* Intrinsic supercurrent diode effect in NbSe<sub>2</sub> nanobridge. *Microstructures* **4**, 2024018 (2024).
- 17. Wickramaratne, D., Khmelevskyi, S., Agterberg, D. F. & Mazin, I. Ising superconductivity and magnetism in NbSe<sub>2</sub>. *Physical Review X* **10**, 041003 (2020).
- 18. Wu, Y., He, J. J., Han, T., Xu, S., Wu, Z., Lin, J., Zhang, T., He, Y. & Wang, N. Induced Ising spin-orbit interaction in metallic thin films on monolayer WSe<sub>2</sub>. *Physical Review B* **99**, 121406 (2019).
- 19. Han, T. *et al.* Investigation of the two-gap superconductivity in a few-layer NbSe<sub>2</sub>-graphene heterojunction. *Physical Review B* **97**, 060505 (2018).
- 20. McHugh, J. G., Enaldiev, V. V. & Fal'ko, V. I. Moiré superstructures in marginally twisted NbSe<sub>2</sub> bilayers. *Physical Review B* **108**, 224111 (2023).
- 21. Oh, M., Nuckolls, K. P., Wong, D., Lee, R. L., Liu, X., Watanabe, K., Taniguchi, T. & Yazdani, A. Evidence for unconventional superconductivity in twisted bilayer graphene. *Nature* **600**, 240–245 (2021).
- 22. Li, T. *et al.* Quantum anomalous Hall effect from intertwined moiré bands. *Nature* **600**, 641–646 (2021).
- 23. Kang, W.-H., Barth, M., Costa, A., Garcia-Ruiz, A., Mreńca-Kolasińska, A., Liu, M.-H. & Kochan, D. Magnetotransport and spin-relaxation signatures of the radial Rashba and Dresselhaus spin-orbit coupling in proximitized graphene. *Physical Review Letters* **133**, 216201 (2024).
- 24. Veneri, A., Perkins, D. T., Péterfalvi, C. G. & Ferreira, A. Twist angle controlled collinear Edelstein effect in van der Waals heterostructures. *Physical Review B* **106**, L081406 (2022).
- 25. Frank, T., Faria Junior, P. E., Zollner, K. & Fabian, J. Emergence of radial Rashba spin-orbit fields in twisted van der Waals heterostructures. *Physical Review B* **109**, L241403 (2024).
- 26. Vodolazov, D. Y. & Peeters, F. Superconducting rectifier based on the asymmetric surface barrier effect. *Physical Review B* **72**, 172508 (2005).
- 27. Sivakov, A., Turutanov, O., Kolinko, A. & Pokhila, A. Spatial characterization of the edge barrier in wide superconducting films. *Low Temperature Physics* **44**, 226–232 (2018).

- 28. Suri, D., Kamra, A., Meier, T. N., Kronseder, M., Belzig, W., Back, C. H. & Strunk, C. Non-reciprocity of vortex-limited critical current in conventional superconducting micro-bridges. *Applied Physics Letters* **121** (2022).
- 29. Bean, C. & Livingston, J. Surface barrier in type-II superconductors. *Physical Review Letters* **12,** 14 (1964).
- 30. Castellani, M., Medeiros, O., Buzzi, A., Foster, R. A., Colangelo, M. & Berggren, K. K. A superconducting full-wave bridge rectifier. *Nature Electronics* **8**, 417–425 (2025).
- 31. Kochan, D. & Strunk, C. Low-loss electronics with superconducting diodes. *Nature Electronics* **8**, 380–381 (2025).
- 32. Bland, J. M. & Altman, D. G. Statistics notes: bootstrap resampling methods. *British Medical Journal* **350** (2015).
- 33. Johansson, J. R., Nation, P. D. & Nori, F. QuTiP: An open-source Python framework for the dynamics of open quantum systems. *Computer Physics Communications* **183**, 1760–1772 (2012).
- 34. Bozkurt, A. M., Brookman, J., Fatemi, V. & Akhmerov, A. R. Double-Fourier engineering of Josephson energy-phase relationships applied to diodes. *SciPost Physics* **15**, 204 (2023).
- 35. Blais, A., Grimsmo, A. L., Girvin, S. M. & Wallraff, A. Circuit quantum electrodynamics. *Reviews of Modern Physics* **93**, 025005 (2021).
- 36. Liu, S., Bordoloi, A., Issokson, J., Levy, I., Vavilov, M. G., Shabani, J. & Manucharyan, V. Strongly-anharmonic gateless gatemon qubits based on InAs/Al 2D heterostructure. *arXiv* preprint arXiv:2503.12288 (2025).
- 37. Leger, P. A., Ramesh, A., Ulloa, T. & Wu, Y. Machine learning enabled fast optical identification and characterization of 2D materials. *Scientific Reports* **14,** 27808 (2024).
- 38. Zhang, B., Lu, P., Tabrizian, R., Feng, P. X.-L. & Wu, Y. 2D Magnetic heterostructures: spintronics and quantum future. *npj Spintronics* **2**, 6 (2024).
- 39. Sosa, L., Wi, M., Barrera, M., Nasrullah, I. & Wu, Y. Simulating Pattern Recognition Using Non-volatile Synapses: MRAM, Ferroelectrics and Magnetic Skyrmions. *Journal of Magnetism and Magnetic Materials* **630**, 173353 (2025).
- 40. Wu, H. *et al.* The field-free Josephson diode in a van der Waals heterostructure. *Nature* **604**, 653–656 (2022).
- 41. Lee, J. *et al.* Twisted van der Waals Josephson junction based on a high- $T_C$  superconductor. *Nano Letters* **21**, 10469–10477 (2021).
- 42. Chen, P. *et al.* Edelstein effect induced superconducting diode effect in inversion symmetry breaking MoTe<sub>2</sub> Josephson junctions. *Advanced Functional Materials* **34**, 2311229 (2024).
- 43. Chen, P. *et al.* Asymmetric edge supercurrents in MoTe<sub>2</sub> Josephson junctions. *Nanoscale Advances* **6**, 690–696 (2024).
- 44. Lyu, Y.-Y. *et al.* Superconducting diode effect via conformal-mapped nanoholes. *Nature communications* **12**, 2703 (2021).

## Acknowledgment

We want to thank Dr. Yasen Hou for help in the experiment setup and meaningful discussions. Support from UF Gatorade award and Research Opportunity Seed Fund are kindly acknowledged. This material is also based upon work supported by the National Science Foundation under Grant No. 2441051 and No. 2501208 (Y. Wu). Partial support from the project IM-2021-26 (SUPER-SPIN) funded by the Slovak Academy of Sciences via the programme IMPULZ 2021, is acknowledged (D. Kochan). This work is supported by the U.S. Department of Energy, Office of Science, Basic Energy Sciences under Award No. DE-SC0004890 (I. Žutić)

## **Author Contributions**

Y. Wu conceived the ideas, supervised the project and led the manuscript writing. H. Zhong led sample fabrication, experiment measurements, data collection and quantum simulations. D. Kochan proposed truncated qubit Hamiltonian, together with I. Žutić they interpreted results and gave theoretical guidance. All authors discussed and commented on the manuscript and also contributed to the manuscript revision.

# **Competing Interests**

The authors declare no other competing interests.

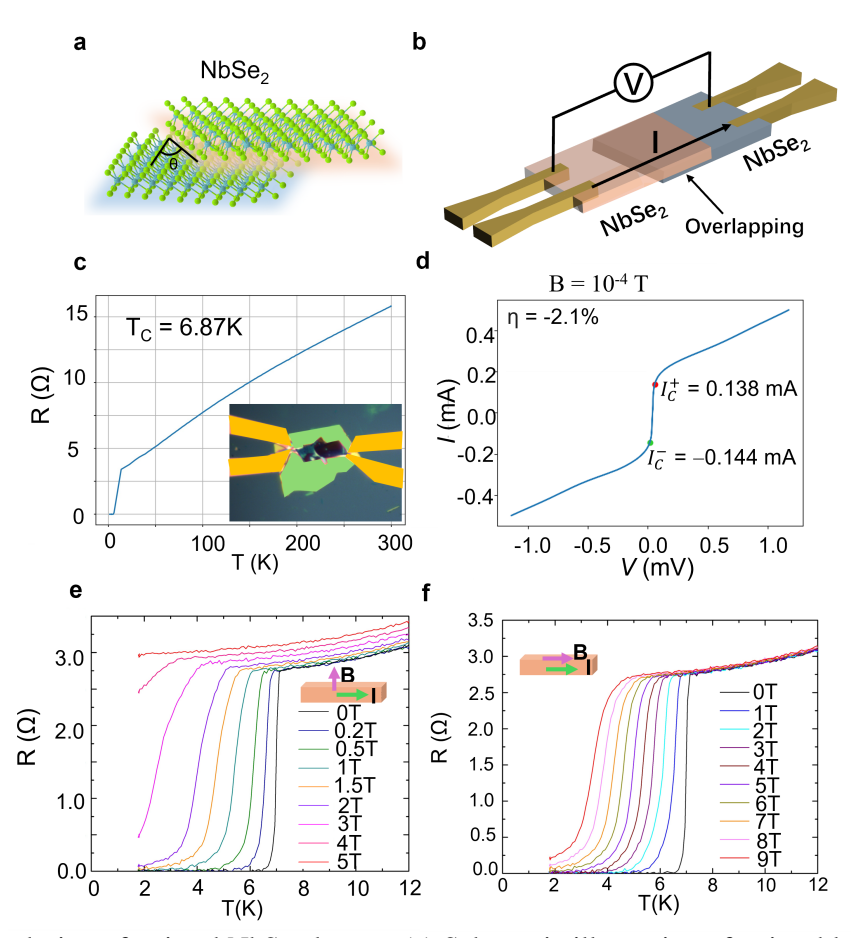


Figure 1: Diode design of twisted NbSe<sub>2</sub> layers. (a) Schematic illustration of twisted layers with an angle  $\theta$ . (b) Current and voltage measurements using four terminal setup. (c) Dependence of the resistance on temperature indicating a critical temperature of 6.87 K. (d) Typical current-voltage characteristics under an applied in-plane magnetic field close to 0 T and determination of the corresponding critical currents  $I_c^+$  and  $I_c^-$ . (e) Out-of-plane and (f) in-plane magnetic field dependence of critical temperature. All data are from a sample with an overall thickness of 16 nm.

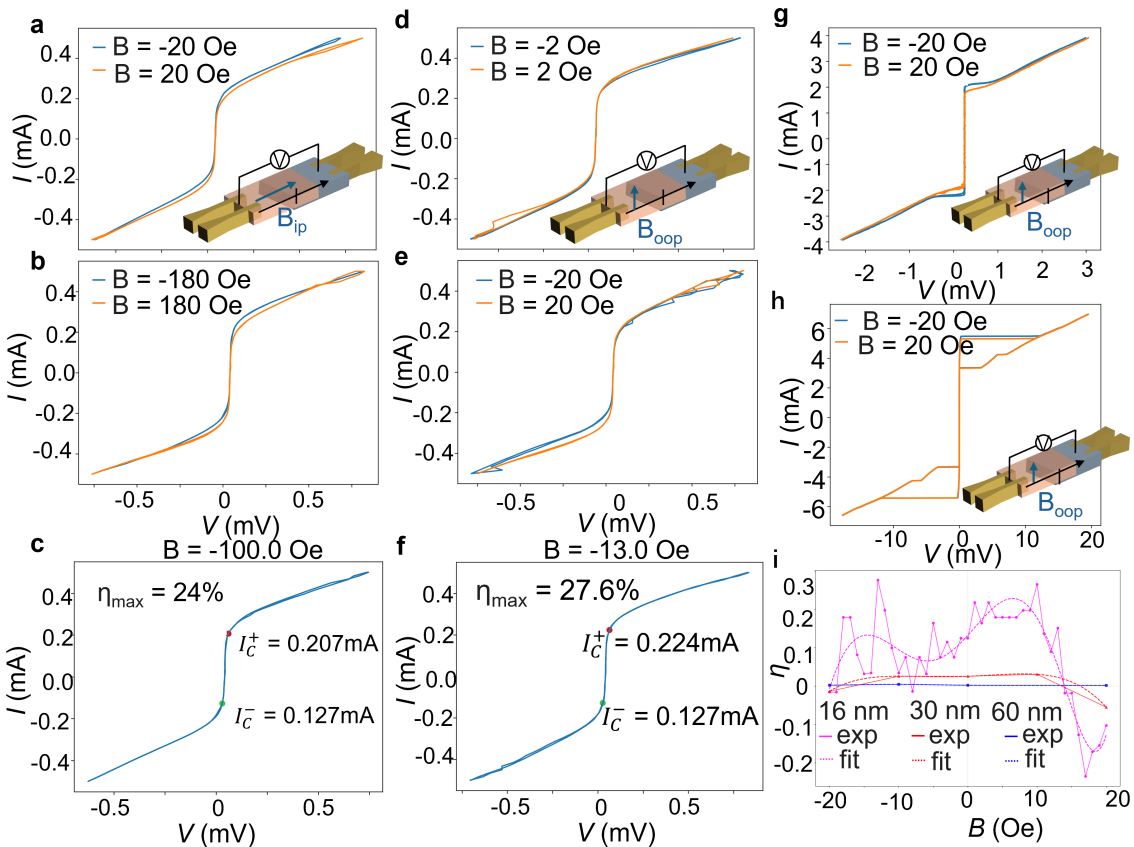


Figure 2: Current-voltage characteristics of the twisted NbSe<sub>2</sub> bilayers with overall thickness of (a-f) 16 nm, (g) 30 nm, and (h) 60 nm. (a) I-V curves under the in-plane magnetic field at -20 Oe and 20 Oe applied along the current. (b) the same as in (a) but at -180 Oe and 180 Oe. (c) In-plane maximum diode efficiency is achieved when the in-plane magnetic field is -100 Oe. (d) I-V curves under the out-of-plane magnetic field at -2 Oe and 2 Oe. (e) the same as in (d) but at -20 Oe and 20 Oe. (f) The maximum diode efficiency is achieved when the out-of-plane magnetic field is -13 Oe. (g) I-V curves under the out-of-plane magnetic field at -20 Oe and 20 Oe for overall 30 nm thick sample. (h) the same as in (g) but for 60 nm thick sample. (i) Diode efficiencies and fittings as functions of the out-of-plane magnetic field B for NbSe<sub>2</sub> junctions with different overall thicknesses: 16 nm (magenta), 30 nm (orange), and 60 nm (blue), see the corresponding color coding.

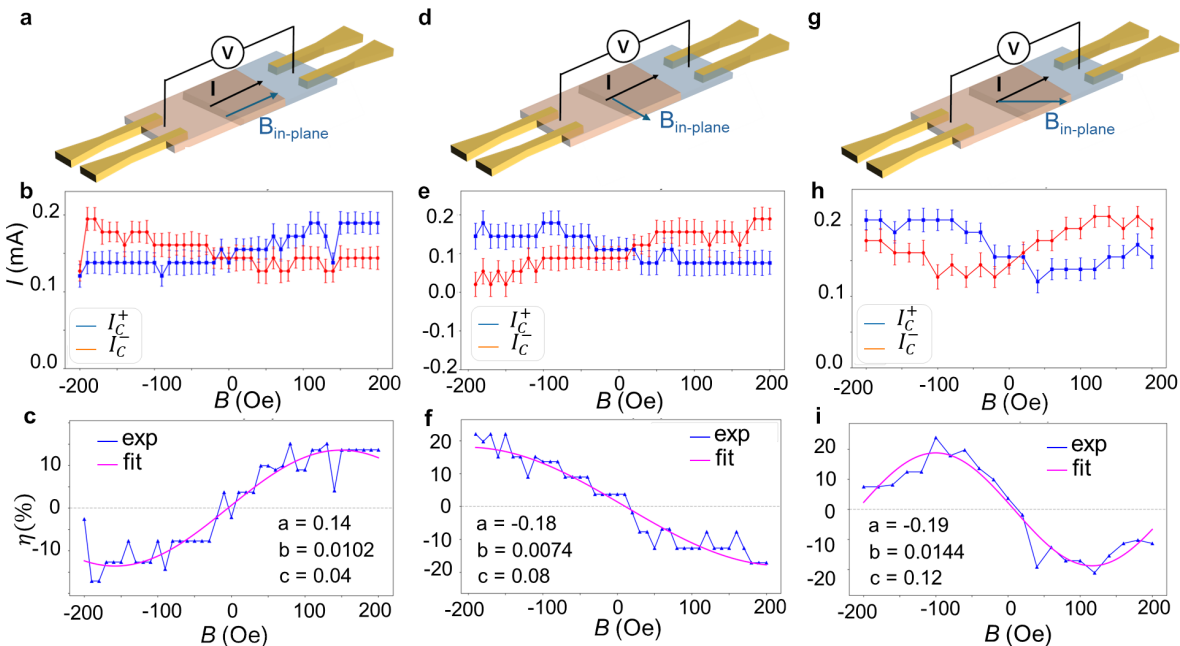


Figure 3: Diode effect for various in-plane magnetic field configurations measured in a sample with overall thickness of 16 nm. (a)-(c) show the magnetic field parallel to the electric current, with the critical current extracted under varying magnetic field strengths in (b), and the diode efficiency as a function of magnetic field in (c). (d)-(f) show the diode characteristics for the in-plane magnetic field perpendicular to the electric current, with the corresponding critical currents extracted in (e) and diode efficiency in (f). (g)-(i) show the same as before for a random in-plane angle between the magnetic field and current, with the critical current in (h) and diode efficiency in (i). Panels (c), (f), and (i) also show the least-squares fitting (fit) of the experimental data (exp) of the diode efficiency  $\eta$ , that is in the range of *B*-field from -200 to 200 Oe following  $\eta = a \cdot \sin(b \cdot B + c)$ , the corresponding values of a, b (in units of inverse Oe) and c are given.

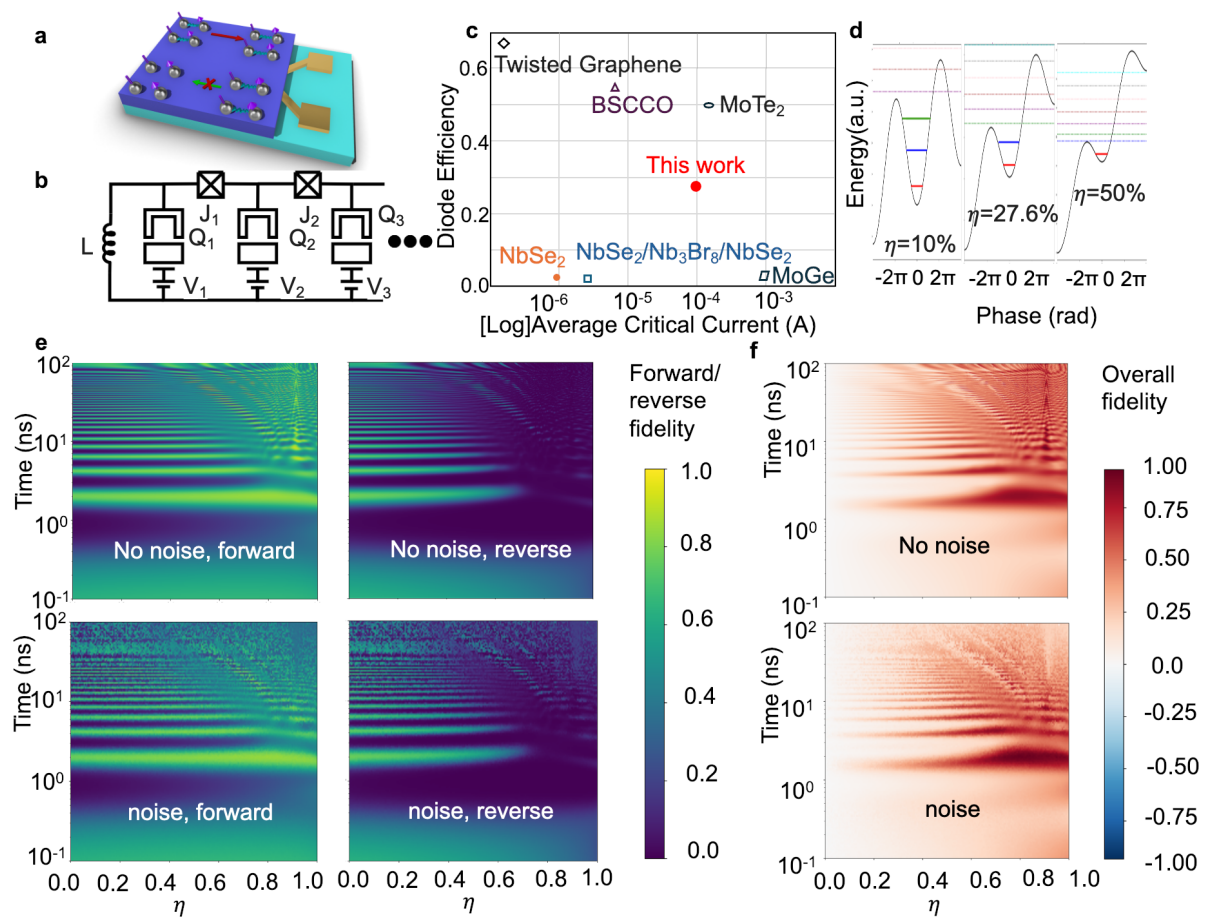


Figure 4: Quantum circuit design and simulation. (a) Schematics of the NbSe<sub>2</sub> device exhibiting a nonreciprocal behavior. (b) Transmon qubit chain circuit with quantum diodes. (c) Benchmark plot comparing diode efficiency and average critical current in reported 2D layered systems, with this work highlighted in red. The efficiencies were calculated from experiments [11, 12, 40–44]. (d) Simulation of the potential-energy landscape with the corresponding energies of the qubit levels inside the quantum wells for the three representative efficiencies  $\eta$ , a perfect two-level system can be achieved for  $\eta$  close to 27.6%. (e) Forward and reverse quantum diode fidelity simulations—as functions of the efficiency and time—without (above) and with (below) noise (based on circuit in (b)). (f) Overall fidelity difference between forward and reverse qubit transfer without (above) and with (below) noise.